VIII International Conference on Fracture Mechanics of Concrete and Concrete Structures
FraMCoS-8
J.G.M. Van Mier, G. Ruiz, C. Andrade, R.C. Yu and X.X. Zhang (Eds)

ASSESSMENT RISK OF FRACTURE IN THIN-WALLED FIBER REINFORCED AND REGULAR HIGH PERFORMANCE CONCRETES SANDWICH ELEMENTS

KAMIL HODICKY[*], THOMAS HULIN[*], JACOB W. SCHMIDT[*] AND HENRIK STANG[*]

[*] Technical University of Denmark (DTU)
Department of Civil Engineering, Section of Structural Engineering
Brovej, Building 118, Kongens Lyngby, DK-2800, Denmark
e-mail: kamh@byg.dtu.dk, www.byg.dtu.dk

Key words: High Performance Concrete, Fiber Reinforced Concrete, Fracture Mechanics, Sandwich Elements, Finite Element Analysis

Abstract: High Performance Concrete Sandwich Elements (HPCSE) are an interesting option for future low or plus energy building construction. Recent research and development work, however, indicate that such elements are prone to structural cracking due to the combined effect of shrinkage and high temperature load. Due to structural restraints, autogenous shrinkage may lead to high self-induced stresses. Therefore autogenous shrinkage plays important role in design of HPCSE.
The present paper assesses risk of fracture due to autogenous shrinkage-induced stresses in three fiber reinforced and regular High Performance Concretes (HPC). The research work described in this paper contains a description of experimental setup that allows measurement of effective shrinkage in HPC, which develops on an elastic inhomogeneity embedded in HPC matrix undergoing shrinkage during hydration (autogenous shrinkage). The test setup is based on direct measurement of the hydrostatic pressure developed in a simple pressure sensor embedded in the same matrix and a subsequent analysis based on Eshelby's solution for an ellipsoidal inhomogeneity embedded in an infinite matrix.
The paper also presents the analysis necessary to perform an interpretation of the experimental results and to determine effective shrinkage in the HPC matrix.
Furthermore, the mechanical properties of all the mixes – static elastic modulus, compression strength, tensile strength as well as fracture energy were investigated in detail as function of time.
Finally the paper describes the modeling work with HPCSE predicting structural cracking provoked by autogenous shrinkage. It was observed that risk of cracking due to autogenous shrinkage rapidly rises after 3 days in case of regular HPC and after 7 days in case of fiber reinforced HPC.

1 INTRODUCTION

Thin-walled High Performance Concrete Sandwich Elements (HPCSE) undergo volume changes. These changes are generated by high thermal load applied on the concrete plates in the hardened state combined with autogenous and drying shrinkage during hardening. HPCSE are particularly sensitive to self-desiccation of the cement paste during hydration process, which leads to autogenous shrinkage. If a restraint is present, autogenous shrinkage may lead to high self-induced stresses [1-3]. In practice, restraint of HPCSE arises from rigid inhomogeneities, reinforcement, temperature gradients over the specimen thickness and subgrade friction that limits the volumetric changes.
The prediction of shrinkage cracking due to restraint is a complex phenomenon dependent on the interaction of several factors such as:

free shrinkage, creep relaxation, material stiffness, fracture resistance, environmental conditions, time dependence, and degree of restraint [4,5]. Autogenous shrinkage should be limited because it may possibly cause surface and even through-thickness micro-craking or macro-cracking and impair the concrete quality [6]. Therefore autogenous shrinkage plays important role in design of HPCSE. The present paper is case study of 3.59m wide and 4.48m high load carring HPCSE. These HPCSE were subjected to structural cracking approximately 6 months after assembly. The HPCSE consist of an internal layer of insulation and two external High Performance Concrete (HPC) plates. The connectors are used to keep the plates together and the panel intact during handling. The prediction of shrinkage cracking is a complex problem dependent on several factors as was already mentioned. The experimental investigations and monitoring of all these factors could lead to high financial cost and long-term measurement.

This work presents a low cost experiment which can combine several factors into one. The experimental work is based on direct measurement of the augoneous shrinkage-induced stresses.

In former studies some experiments of self-induced stresses in concrete were performed. Nielsen [7] in his doctoral study developed a stress sensor to measure the stresses in an aggregate in a uniaxial creep test. The technique of measurement was based on change in the mutual inductance between two coils which are displaced in relation to each other. Furthermore, Sato et al. [8] attempted to measure self-induced stress with an embedded deformed bar and inspection of micro-crack in concrete at the vicinity of rebar. Dela [9] used massive porcelain spheres encircled with manganin wire glued to the surface as stress sensor to predict the magnitude of eigenstresses around aggregates in hardening cement paste. Her study is based on linear elastic solution and stepwise calculation taking into account change in the stiffness but disregarding the relaxation. Finally, the work by Stang [10] should be mentioned. In this work, the shrinkage-induced clamping pressure acting on aggregates and different fiber types embedded in cement pastes were investigated as a function of time. The estimation is based on direct measurement of the pressure developed in a simple pressure sensor embedded in the same matrix and a subsequent analysis based on Eshelby's solution [11] for an ellipsoidal inhomogeneity embedded in an infinite matrix.

The main motivation of the present work is to demonstrate that autogenous shrinkage of the HPC contributes to the potential structural cracking of the front plate of the HPCSE. Three fiber reinforced and regular HPC mixes were analyzed in order to assess risk of fracture and eventually foresee whether cracks will be propagated stably or unstably. Additionally the mechanical properties of all mixes – Static elastic modulus, compressive strength, tensile strength as well as fracture energy were investigated in detail as function of time.

2 EXPERIMENTAL PROCEDURE

The present work represents three fiber reinforced and regular HPC mixes. The first mix was a commercial mix developed by CONTEC ApS and will be denoted as Contec mix. Another two HPC mix designs were based on research work of Ozbay et al. [12]. These two mixes were denoted as DTU mixes. The DTUI mix was designed to correspond to the mechanical properties of the Contec mix. The DTUII mix was adjusted by bauxite sand and fly ash to obtain better mechanical properties than Contec and DTUI. The mix designs are shown in Table 1.

A 60l pan mixer was used for mixing; mixing time was 2 minutes for the dry mixing and 5 minutes with water and super-plasticizer. The vibrating time was chosen to be 30s. After casting, the specimens were left to harden in a climate chamber (22±2 °C and 65±5% RH). Specimens were demoulded after 24h and put in the water at 20 °C for curing.

Beams for determination of the mechanical properties were casted in one use polystyrene moulds.

Table 1 – HPC mix designs (kg/m^3)

Mix	Contec	DTUI	DTUII	Contec-F	DTUIF	DTUIIF
Cement (CEM I 52.5 R)	/	495	460	/	495	460
Binder Contop S 105-2	582.3	/	/	582.3	/	/
CA, granite, 02-05 mm	832.3	868.4	1015.6	832.3	868.4	1015.6
FA, sea gravel, 0.1-1.5 mm	763.7	781.6	/	763.7	781.6	/
FA, bauxite sand, 0-1 mm	/	/	609.4	/	/	609.4
Silica fume	/	55	57.5	/	55	57.5
Fly ash	/	/	57.5	/	/	57.5
Super-plasticizer	/	11	25.9	/	11	25.9
Glass fibers	/	/	/	4.04	4.0	3.5
Polypropylene fibers	/	/	/	2.02	2.0	1.78
Total dry mass	2178.3	2200	2200	2184.4	2206	2205.3
Water-cementitious material ratio	0.304	0.25	0.25	0.304	0.25	0.25
Water-cementitious material ratio*	/	0.27	0.295	/	0.27	0.295

* including the water content of the superplasticizer

3 MECHANICAL PROPERTIES

The developments of the mechanical properties - Static elastic modulus, compression strength, tensile strength (wedge splitting test) as well as fracture energy were investigated in detail as function of time. All the tests were performed at room temperature (20±2 °C). The compressive strength and static elastic modulus were determined according to EN 1992-1-1 [13]. Specimen geometry for mechanical tests is shown in Table 2.

Table 2 – Specimen geometry for different tests

Test	Specimen geometry
Compressive strength	W/H/L = 40/40/40 mm
Tensile strength	W/H/L = 100/100/100 mm
Static elastic modulus	W/H/L = 100/100/100 mm

3.1 Compressive strength

The mean compressive strength at 28 days was observed to range roughly between 75 to 110 MPa. DTU mixes have significantly higher development of compressive strength during the first days. This phenomena can be explained by the use of the cement with rapid hardening together with silica fume and fly ash in case of DTUII(F). There was not found any significant difference in compressive strength between regular HPC mixes and the fiber reinforced. Development of compression strength for all HPC mixes is shown in Table 3.

3.2 Tensile strength

The 28 days splitting tensile strength of all HPC mixes was high around 5.5 MPa. The tensile strength of the DTU mixes made with silica fume, fly ash and cement with rapid hardening was observed to develop faster. After three days it was at roughly 5 MPa - well above the strength of the Contec mixes, 3 MPa (Table 3). Tensile strength development of Contec mixes tended to increase slower than DTU mixes. There was no obvious change of tensile strength caused by adding fibers to HPC matrix.

3.3 Static elastic modulus

With the exception of the Contec mixes, the mean static elastic modulus of the concretes E_{cm}, reached about 60GPa after 28 days. The static elastic modulus of the Contec mixes was at 40GPa, thus significantly lower. This seems to be caused by discontinues grain size distribution curve and by a disadvantageous pore size distribution of the hardened concrete. The static elastic modulus of the DTU mixes developed significantly faster than Contec mixes (Table 3).

3.4 Fracture energy

An experimental investigation completed as part of this study were using the Wedge splitting test (WST) to ascertain the fracture behaviour of the concrete mixtures used

throughout this work. The specimen geometry and analysis needed to evaluate the WST were published in Ref. [14]. The fracture energy G_f, characterize the material's resistance to fracture. The mean fracture energy G_{fm}, was found to increasing with age for all the mixes. The brittleness of cohesive material can be described by the characteristic length, L_{ch}. The general trend in the development of the mean characteristic length L_{chm}, was observed to decrease with maturity. The same results were also found in literature, e.g. [15-16].

Table 3 – Mechanical properties

Mix	Age (days)	$f_{cm,cube}$ – SD (MPa)	$f_{ctm,sp}$ – SD (MPa)	E_{cm} – SD (GPa)	L_{chm} – SD (mm)	G_{fm} – SD (N/m)
Contec	1	31.4 – 4.8	2.1 – 0.0	41.3 – 0.8	777 – 89	81.5 – 7.6
	3	43.6 – 8.2	3.0 – 0.4	43.7 – 5.8	430 – 109	86.1 – 35.2
	7	59.1 – 3.2	5.1 – 0.9	36.5 – 1.4	115 – 24	110.6 – 8.2
	28	72.3 – 8.4	5.2 – 2.1	43.3 – 0.0	186 – 49	115.9 – 1.4
DTUI	1	61.5 – 3.5	3.6 – 0.4	53.5 – 0.5	768 – 48	182.7 – 22.6
	3	65.6 – 2.2	4.4 – 0.0	44.9 – 7.5	281 – 3	119.8 – 19.5
	7	73.1 – 6.9	5.6 – 0.3	60.0 – 6.0	234 – 34	124.3 – 17.2
	28	89.2 – 3.7	6.5 – 1.4	55.5 – 11.6	168 – 29	129.3 – 8.0
DTUII	1	60.9 – 10.2	2.9 – 0.6	43.5 – 1.5	621 – 167	116.4 – 27.1
	3	81.8 – 4.3	4.7 – 0.1	48.3 – 3.1	234 – 14	106.0 – 2.9
	7	84.2 – 6.3	4.9 – 0.0	53.8 – 7.8	279 – 79	121.9 – 9.5
	28	102.7 – 9.0	5.5 – 0.6	58.6 – 19.0	258 – 4	134.6 – 2.4
Contec-F	1	38.0 – 5.2	2.1 – 0.3	39.1 – 0.5	1652 – 188	184.8 – 9.7
	3	52.1 – 2.5	3.3 – 0.4	36.5 – 0.4	464 – 76	136.5 – 7.4
	7	60.3 – 4.0	3.9 – 0.0	36.4 – 0.9	370 – 14	157.8 – 4.4
	28	71.9 – 1.5	4.6 – 0.6	35.0 – 4.9	346 – 156	204.8 – 5.7
DTUIF	1	47.4 – 3.5	3.4 – 0.1	50.0 – 1.1	697 – 60	158.2 – 11.8
	3	64.9 – 5.8	4.8 – 0.2	48.5 – 0.6	344 – 54	161.0 – 4.2
	7	65.0 – 5.4	5.9 – 0.2	43.3 – 10.4	209 – 3	167.8 – 20.6
	28	81.6 – 2.3	6.5 – 0.5	52.3 – 5.6	223 – 156	168.9 – 29.1
DTUIIF	1	58.1 – 7.3	3.5 – 0.1	48.1 – 1.5	894 – 76	222.5 – 40.1
	3	75.1 – 5.8	5.0 – 0.0	46.8 – 1.6	299 – 42	157.0 – 7.8
	7	83.8 – 5.3	5.1 – 1.7	46.8 – 2.1	245 – 25	135.8 – 14.8
	28	111.9 – 4.6	5.2 – 0.2	58.7 – 0. 1	338 – 21	155.8 – 3.7

3.5 Autogenous shrinkage-induced stresses

The experimental setup proposed by Stang [10] was used to determine autogenous shrinkage-induced stresses. As stress sensor a laboratory mercury thermometer with temperature scale going from 0 to 50°C and a precision of 0.1°C was chosen. The stress sensors were calibrated for hydrostatic pressure by using the so-called Budenberg instrument. The Budenberg was loaded stepwise until reaching 50 bars, and then unloaded. The average calibration factor α, was found to be 1.67MPa/°C. Furthermore, the amount of mercury in the capillary tube was measured by weighing the tube with and without mercury and the calibration factor β (g/°C), was determined related to apparent temperature change to mass of mercury. The equivalent compression modulus of the stress sensor κ^e, was determined according Eq. 1:

$$\kappa^e = \frac{\alpha \gamma_{hg}}{\beta} \nu \tag{1}$$

where γ_{hg} is density of mercury and ν is the total volume of mercury cell (glass and mercury). Based on modelling the mercury cell as an axis-symmetric ellipsoidal shell with wall thickness h, the linear elastic solution for the equivalent compression modulus κ^{e*}, can be determined as shown in Eq.2 [10]

$$\kappa^{e*} = \frac{2E^s h}{3bI} \qquad (2)$$

where E^s is static elastic modulus and I is function of a/b (a is the length of the half-axis in the direction of symmetry and b is radius of the cell) and Poisson's ration v^s.
The calculated bulk moduli based on linear elastic shell solution were compared with measured one. It was found that results of measured and calculated bulk moduli, κ^e and κ^{e*}, are close with 10% differences between them.

To record properly the stresses due to autogenous shrinkage, the thermometer should disturb the concrete as little as possible. The glass tube protecting the mercury-filled capillary is removed leaving only the mercury container and the capillary (see Fig. 1a). Before casting, the 18 cylinders (3cylinders per mix) were oiled to allow the HPC freely shrink without applying tension on the cylinder. After calibration, the stress sensors were casted into the center of PVC cylindrical mould filled with the HPC. The cylinders had a diameter of 100mm and a height of 200mm. The recording of the temperature during long-term testing was performed by thermocouples inserted in the concrete cylinder. To compensate the 0.2°C precision
of the couples, two couples were inserted close to the thermometer and the average of their readings was considered. After casting, the top of the cylinder was covered with a thin layer of oil to preserve the water from evaporating (see Fig. 1b) Thus, the HPC experience only autogeneous shrinkage and temperature variation associated with the hydration process.

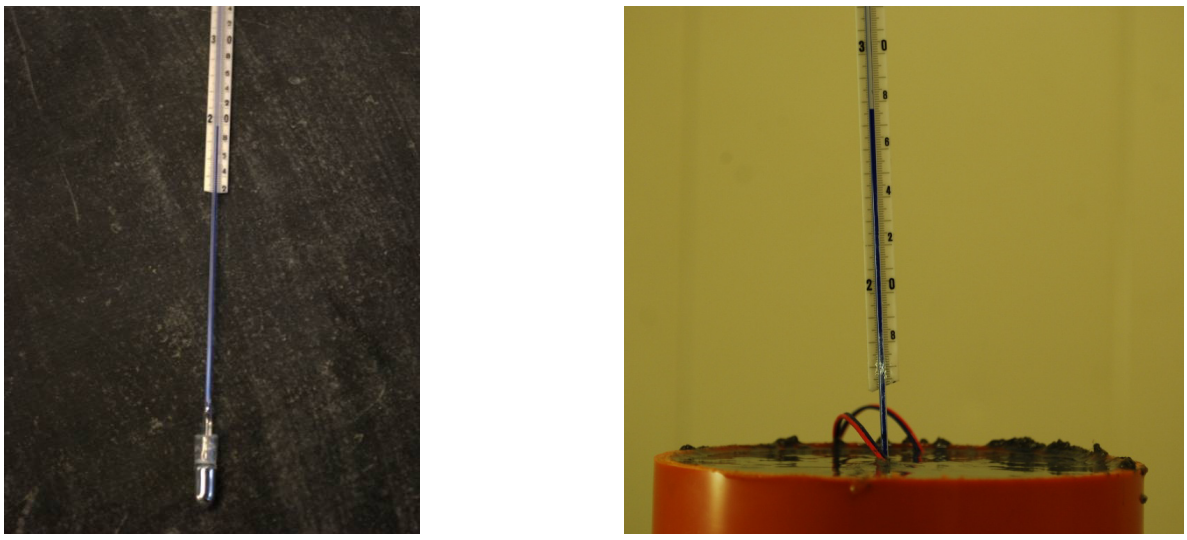

(a) (b)

Figure 1: a) Photograph showing the different parts of the mercury thermometer used as a pressure sensor in the experimental investigations. b) Photograph showing the experimental setup, the PVC mould, the stripped thermometer, and the thermocouple module.

The output of observation was based on temperature differences ΔT, between the stress sensor and average value of the two thermocouples observed over time t, where t = 0 corresponds to the beginning of experiment (30 minutes after mixing). Using the calibration factor α, the observed ΔT was readily transformed to an equivalent hydrostatic stress state σ^e_{hyd}, in the equivalent elastic inhomogeneity:

$$\sigma^e_{hyd}(t) = \alpha(\Delta T(t) - \Delta T(t=0)) \qquad (3)$$

The development in equivalent hydrostatic stress state for six different mixes is shown in Fig. 2. Figure 2 clearly shows that there is a significant difference between the DTU and Contec mixes. A much higher hydrostatic stress develops in the sensors embedded

in DTU mixes. Furthermore, the hydrostatic stress keeps rising in the Contec mixes and then after approximately 600 hours drops to an almost constant level. The hydrostatic stress of the DTU mixes keeps constantly rising up to 2000 hours then the curve is flattened. All fiber reinforced mixes showed the same tendency in development of the hydrostatic stresses as regular HPC mixes. However, there is a lack of information in literature whether increase of the hydrostatic stresses in fiber reinforced HPC mixes is significant or not. The experimental programme with more specimens would be necessary to statistically confirm this phenomenon.

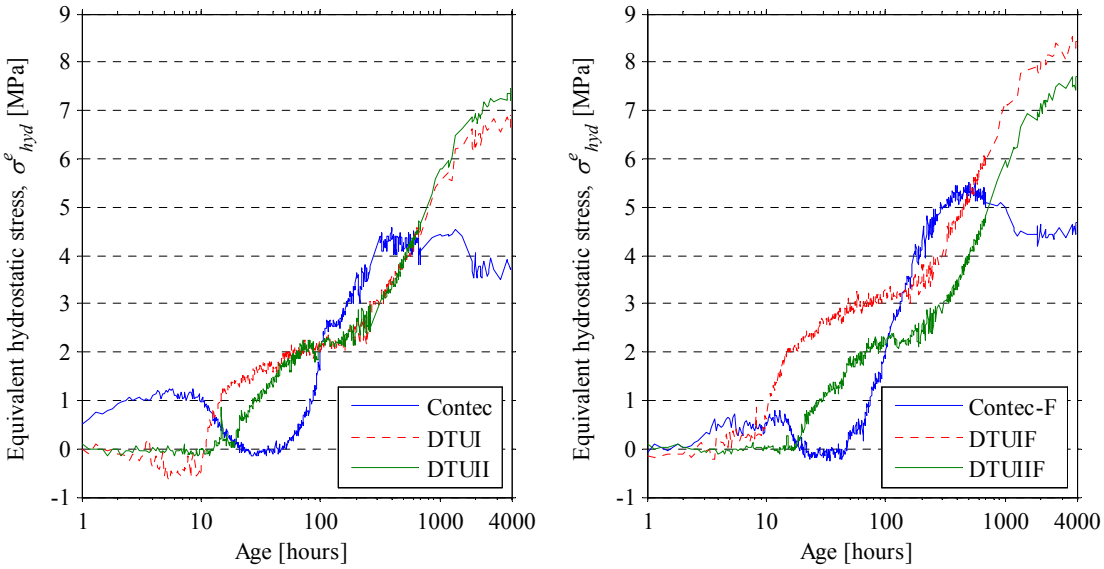

Figure 2: Development in equivalent hydrostatic stress σ^e_{hyd}, in the pressure sensors.

The analysis in ref. [10] based on Eshelby's original superposition scheme [11] with homogeneous infinite medium and an inclusion undergoing a stress-free strain was utilized in interpretation of the experimental results. The concept of effective shrinkage $\varepsilon^{s,e}$, was defined as a function of time according Eq. 4. The effective shrinkage can be defined as the autogenous shrinkage that in linear elastic system interpret the correct stress state in an embedded equivalent inhomogeneity.

$$\varepsilon^{s,e}(t) = \frac{\sigma^e_{hyd}(t)}{E_c(t)}\left(\frac{1+\upsilon_c}{1+\upsilon_i} + \frac{E_c(t)}{3\kappa^{e*}}\right) \qquad (4)$$

Here $E_c(t)$ is static elastic modulus of the HPC mixes as function of time. The Poisson's ratio of the HPC mixes, υ_c of 0.2, is assumed to be equal to Poisson's ratio of embedded inhomogeneity, υ_i.

Looking at Figure 3, it has to be noted that static elastic modulus of the HPC mixes was measured at certain time steps of maturity as shown in Table 3. To build up the effective shrinkage curves, the static elastic modulus of the HPC mixes as function of time was linearly interpolated between the measured ones. The effective shrinkage of the Contec mixes rises to 2.5 10^{-4}- 3.0 10^{-4} and after approximately 600 hours drops to an almost constant level of about 2.0 10^{-4}- 2.5 10^{-4}. The significant drop can be explained by relaxation, which plays an important role in Contec mixes. In the case of the DTU mixes the effective shrinkage keeps rising, however, with a much lower rate. The effective shrinkage at 4000 hours almost reaches double of the Contec mixes, about 3.0 10^{-4}- 4.0 10^{-4}.

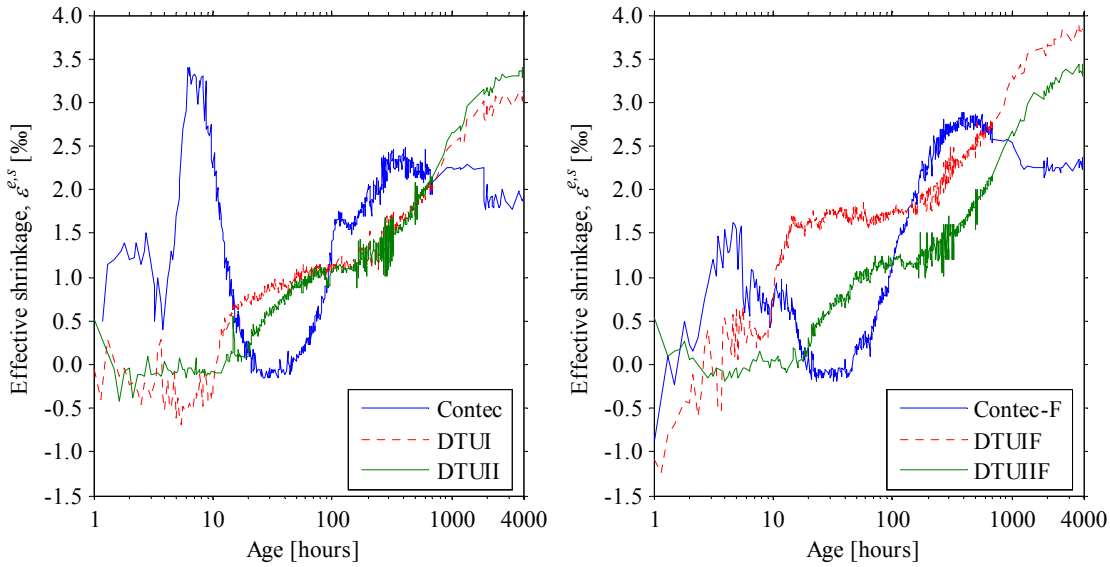

Figure 3: Development in effective shrinkage, $\varepsilon^{s,e}$ for different inhomogeneities.

4 ASSESSMENT RISK OF FRACTURE

In the case of HPCSE embedded steel connectors cause restrain to the HPC plates, see Fig. 4. The finite element program Abaqus was used to calculate the response of the concrete front plate to autogenous shrinkage. The plate has a width of 3.584m and a height of 4.48m. The thickness of the plate is 20mm. The shear connectors were implemented in the middle of the plate thickness. The calculations made the assumption of linear elastic behaviour/small displacements. A quarter of the panel was modelled, accounting for symmetry. The numerical model consists of two types of element: C3D8T: An 8-node thermally coupled brick for concrete front plate and T3D2T: A 2-node 3-D thermally coupled truss for welded wire truss shear connectors. All the investigated mixes were analyzed in order to assess risk of fracture and eventually foresee weather crack will be propagated stably or unstably. The material data from experiments (Static elastic modulus, E, and coefficient of thermal expansion for HPC mixes, α_c) were used as input to the Abaqus model.

To obtain the right response of the front plate, the analysis has to include autogeneous shrinkage of the front plate as well as an effect of differential shrinkage between front plate and back plate. The effect of differential shrinkage between front plate and back plate was extracted from experimental setup in Section 3.5 as the largest effective shrinkage difference between 3 cylinders of the same mix. The load induced by autogenous shrinkage was applied homogenously over the plate. In order to model autogenous shrinkage, this can be achieved using an extension of Hooke's law for temperature as:

$$\Delta T = \frac{\varepsilon^{s,e}(t)}{\alpha_c} \tag{5}$$

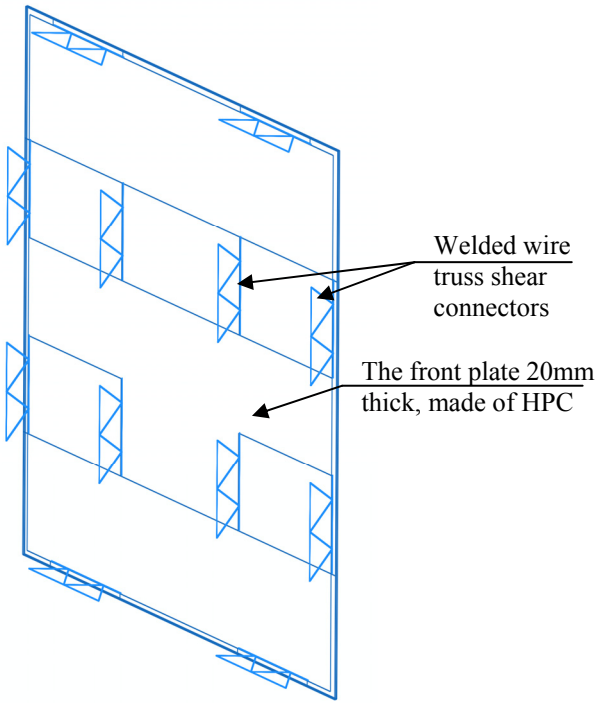

Figure 4: The front plate with an arrangement of the shear connectors.

The models were analyzed for the same maturity as fracture properties were investigated. All of the results showed stresses exceeded the tensile capacity of concrete. The stress distribution was found to be highly localized in vicinity of shear connectors. These highly localized areas can correspond to the crack opening in the infinite sheet. Stang et al. [17] performed a numerical investigation on crack propagation in an infinite sheet for a material with a linear cohesive law. They observed that a crack propagates stably as long as the crack length is smaller than characteristic length, L_{ch}. For larger crack length the crack growth becomes unstable. Dick-Nielsen [18] study illustrates the development of the crack opening and showed that magnitude of the stable crack opening is approximately 5μm, thus very fine crack, which is not visible for human eye. This knowledge was used as first order approximation that linear elastic stresses will introduce crack. To predict the behaviour of the crack, the gray areas were compared with the characteristic lengths shown in Table 3. The crack propagation in the front plate for all the mixes was summarized in Table 4.

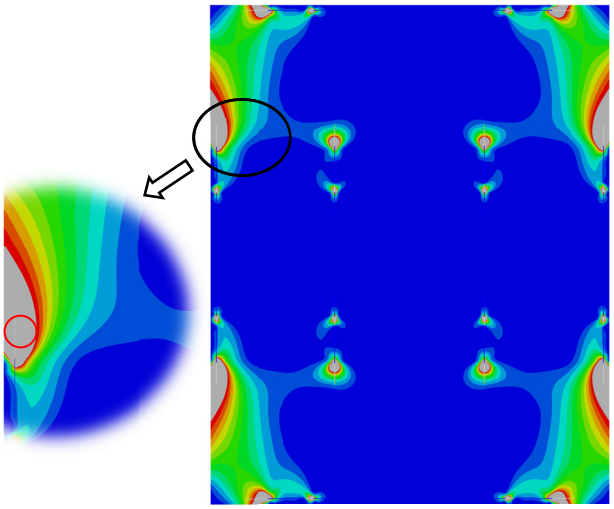

Figure 5: Output of 3D FE-analysis for DTUIF mix at 28 days.

In Fig. 5 is shown example of output of 3D FE-analysis for DTUIF mix at 28 days maturity. The splitting tensile strength for DTUIF mix was set up to 6.5MPa (see Table 3). The red circle in the Fig. 5 depicts the characteristic length which is in this case smaller than area where the tensile strength of concrete is exceeded. This observation leads to prediction that the cracks propagates unstably.

Table 4 – The crack propagation in the front plate

Mix	Age (days)	Crack propagation in the front plate
Contec	1	stable
	3	stable
	7	unstable
	28	unstable
DTUI	1	stable
	3	stable
	7	unstable
	28	unstable
DTUII	1	stable
	3	unstable
	7	unstable
	28	unstable
Contec-F	1	stable
	3	stable
	7	stable
	28	unstable
DTUIF	1	stable
	3	stable
	7	unstable
	28	unstable
DTUIIF	1	stable
	3	stable
	7	stable
	28	unstable

5 CONCLUSIONS

The main assumption motivating this work is that a combination of autogenous shrinkage of the concrete and thermal load from the outside environment could lead to the cracking of the front plate of the HPCSE. In this paper, the risk of cracking related to autogenous shrinkage of the HPCSE made using three fiber reinforced and regular HPC was investigated. In the laboratory, different investigations were carried out in order to determine the characteristics of the concrete to be used as an input for the modelling work. The laboratory experiments and modelling work predicts the risk of cracking and crack propagation with relatively simple means by using the characteristic lengths. The combination of experimental and

modelling work leads to the present conclusions.

The risk of cracking due to autogenous shrinkage rapidly rises after 3 days in case of regular HPC mixes and after 7 days in case of mixes with fibers. The stresses due to autogenous shrinkage have a large role to play also but minor compared to the one of the environmental conditions. The combination of autogenous shrinkage and thermal load from outside environment may lead to massive structural cracking. Furthermore, the stiffness of the shear connectors have a significant role in design of HPCSE. Therefore their stiffness should be studied in detail and new types of shear connector for HPCSE should be developed to avoid of structural cracking.

REFERENCES

[1] Sule, M., Breugel, K.v., 2004. The effect of reinforcement on early-age cracking due to autogenous shrinkage and thermal effects, *Cement and Concrete Composites*, Volume 26, Issue 5, pp. 581–587.

[2] Gilbert, R.I., 2001. Shrinkage, Cracking and Deflection - the Serviceability of Concrete Structures, *Electronic Journal of Structural Engineering*, Vol. 1, No.1, pp. 2-14.

[3] Maruyama, I., Kameta, S., Suzuki, M., Sato, R., 2006. Cracking of high strength concrete around deformed reinforcing bar due to shrinkage, *Int. RILEM-JCI Seminar on Concrete Durability and Service Life Planning*, edited by K. Kovler, RILEM Publications S. A. R. L., Ein-Bokek, Israel, pp.104-111.

[4] Shah, S. P., and Weiss, W. J. and Yang, W., 1997. Shrinkage cracking in High Performance Concrete, *Proceedings of the PCI/FHWA International Symposium on High Performance Concrete,* New Orleans, pp. 148-158.

[5] Shah, S. P. and Weiss, W. J., 2000. High Strength Concrete: Strength, Permeability, and Cracking, *Proceedings of the PCI/FHWA International Symposium on High Performance Concrete,* Orlando, Florida, pp. 331-340

[6] Lura, P., Jensen, O.M., Breugel, K.v., 2003. Autogenous shrinkage in high-performance cement paste: An evaluation of basic mechanisms, *Cement and Concrete research* (ISSN: 0008-8846), Vol: 33, issue: 2, pp: 223-232.

[7] Nielsen, K. E., 1971. Aggregate Stresses in Concrete, PhD thesis, Royal Institute of Technology, Stockholm.

[8] Sato, R., Xu, M., and Yang, Y., 1999. Stresses due to autogenous shrinkage in high strength concrete and its prediction, *Autogesous Shrinkage of Concrete* edited by Tazawa, E., pp. 351-362.

[9] Dela, B.F., 2000. Eigenstresses in Hardening Concrete, Doctoral thesis, Department of Structural Engineering and Materials, Technical University of Denmark.

[10] Stang, H., 1996. Significance of shrinkage-induced clamping pressure in fibre-matrix bonding in cementitious composite materials, *Advanced Cement Based Materials 4*, pp.106-115.

[11] Eshelby, J.D., 1957. The determination of the elastic field of an ellipsoidal inclusion, and related problems, *Proc. R. Soc. Lond*., *A241*, pp. 376-396.

[12] Ozbay, E., Gesoglu, M. and Guneyisi, E., 2011. Transport properties based multi-objective mix proportioning optimization of high performance concretes, *Materials and Structures*, Vol.44, pp.139-154.

[13] Bamforth, P., Chisholm, D., Gibbs, J. and Harrison, T., 2008. Properties of Concrete for use in Eurocode 2, *The Concrete Centre*, ISBN 978-1-904482-39-0.

[14] Skocek, J., and Stang, H., 2008 Inverse analysis of the wedge splitting test, *Engineering Fracture Mechanics*, Vol. 75 (10), pp. 3173–3188.

[15] Østergaard, L., Lange, D. and Stang, H., 2004. Early-age stress–crack opening relationships for high performance concrete, *Cement and Concrete Composites*,Volume 26, Issue 5, pp. 563-572.

[16] Hariri, K. 2000. Bruchmechanisches Verhalten jungen Betons. Laser-Speckle-Interferometrie und Modellierung der Rißprozeßzone, *Deutscher Auss-chuß fur Stahlbeton*, Number 509.

[17] Stang, H., Olesen, J.F., Poulsen, P.N. and Dick-Nielsen, L., 2007. On the application of cohesive crack modeling in cementitious material, *Materials and Structures*, Vol.40, pp. 365-374.

[18] Dick-Nielsen, L., 2008. Modeling of ECC Materials using Numerical Formulations based on Plasticity, PhD thesis, Technical University of Denmark, ISBN: 9788778772435, ISSN: 1601-2917.